IJMMM International Journal of Minerals, Metallurgy and Materials 矿物冶金与材料学报（英文版）

Comparative characterization of iridium loading on catalyst assessment under different conditions

Zahra Amirsardari, Akram Dourani, Mohamad Ali Amirifar, and Nooredin Ghadiri Massoom

Cite this article as:
Zahra Amirsardari, Akram Dourani, Mohamad Ali Amirifar, and Nooredin Ghadiri Massoom, Comparative characterization of iridium loading on catalyst assessment under different conditions, *Int. J. Miner. Metall. Mater.*, 28(2021), No. 7, pp. 1233-1239. https://doi.org/10.1007/s12613-020-2058-4

View the article online at SpringerLink or IJMMM Webpage.

Articles you may be interested in

Zhi-sheng Nong, Hao-yu Wang, and Jing-chuan Zhu, First-principles calculations of structural, elastic and electronic properties of $(TaNb)_{0.67}(HfZrTi)_{0.33}$ high-entropy alloy under high pressure, *Int. J. Miner. Metall. Mater.*, 27(2020), No. 10, pp. 1405-1414. https://doi.org/10.1007/s12613-020-2095-z

Chong Lin, Shu-sen Wu, Shu-lin Lü, Ping An, and He-bao Wu, Effects of high-pressure rheo-squeeze casting on the Fe-rich phases and mechanical properties of Al-17Si-(1,1.5)Fe alloys, *Int. J. Miner. Metall. Mater.*, 25(2018), No. 9, pp. 1018-1026. https://doi.org/10.1007/s12613-018-1652-1

Long Meng, Zhan-cheng Guo, Jing-kui Qu, Tao Qi, Qiang Guo, Gui-hua Hou, Peng-yu Dong, and Xin-guo Xi, Synthesis and characterization of Co_3O_4 prepared from atmospheric pressure acid leach liquors of nickel laterite ores, *Int. J. Miner. Metall. Mater.*, 25(2018), No. 1, pp. 20-27. https://doi.org/10.1007/s12613-018-1542-6

Zhuo Yi, Wen-zhi Fu, Ming-zhe Li, Rui Li, Liang Zhao, and Li-yan Wang, Numerical simulation and experimental verification of a novel double-layered split die for high-pressure apparatus used for synthesizing superhard materials, *Int. J. Miner. Metall. Mater.*, 26(2019), No. 3, pp. 377-385. https://doi.org/10.1007/s12613-019-1747-3

Revanna Kullaiah, Liju Elias, and Ampar Chitharanjan Hegde, Effect of TiO_2 nanoparticles on hydrogen evolution reaction activity of Ni coatings, *Int. J. Miner. Metall. Mater.*, 25(2018), No. 4, pp. 472-479. https://doi.org/10.1007/s12613-018-1593-8

Fabiane Carvalho Ballotin, Mayra Nascimento, Sara Silveira Vieira, Alexandre Carvalho Bertoli, Ottávio Carmignano, Ana Paula de Carvalho Teixeira, and Rochel Montero Lago, Natural Mg silicates with different structures and morphologies: Reaction with K to produce K_2MgSiO_4 catalyst for biodiesel production, *Int. J. Miner. Metall. Mater.*, 27(2020), No. 1, pp. 46-54. https://doi.org/10.1007/s12613-019-1891-9

IJMMM WeChat

QQ author group

International Journal of Minerals, Metallurgy and Materials
Volume 28, Number 7, July 2021, Page 1233
https://doi.org/10.1007/s12613-020-2058-4

Comparative characterization of iridium loading on catalyst assessment under different conditions

Zahra Amirsardari, Akram Dourani, Mohamad Ali Amirifar, and Nooredin Ghadiri Massoom

Space Transportation Research Institute, Iranian Space Research Center, Tehran, Iran
(Received: 8 January 2020; revised: 20 March 2020; accepted: 30 March 2020)

Abstract: To discuss the potential role of iridium (Ir) nanoparticles loaded under atmospheric and high pressures, we prepared a series of catalysts with the same active phase but different contents of 10wt%, 20wt%, and 30wt% on gamma-alumina for decomposition of hydrazine. Under atmospheric pressure, the performance of the catalyst was better when 30wt% of the Ir nanoparticles was used with chelating agent that had greater selectivity of approximately 27%. The increase in the reaction rate from 175 to 220 h^{-1} at higher Ir loading (30wt%) was due to a good dispersion of high-number active phases rather than an agglomeration surface. As a satisfactory result of this investigation at high pressure, Ir catalysts with different weight percentages showed the same stability against crushing and activity with a characteristic velocity of approximately 1300 m/s.

Keywords: iridium nanoparticles; catalyst activity; laboratory reactor; atmospheric pressure; high pressure

1. Introduction

Supported noble metal catalysts are widely used for a variety of catalytic reactions [1]. Iridium (Ir) active-phase catalysts are used to decompose hydrazine [2] in a complex manner. Despite efforts in this field, the catalytic mechanism of hydrazine decomposition and its related factors need further study. Depending on surface species, specific reaction pathways may change. Intermediates and some neighboring Ir atoms are important due to various forms of hydrazine adsorption on the Ir atoms and transition states [3].

Stability without loss of activity is one of the main features of the catalyst, which affects the system lifetime [4]. The decomposition of hydrazine has been conducted on the catalyst with a strong structure, which is capable of stabilizing the system without significant loss [5]. Materials with high thermal conductivity and heat resistant in body structure or part of the catalysts play an important role in the system lifetime [6–8]. The catalyst is stressed on the processing temperatures [9]. Cracks can be created in the granules under these conditions [10]. In porous catalysts based on alumina, temperature gradients are created due to low thermal conductivity. Higher thermal conductivity caused by increased loading of nanoparticles speeds up the spread of heat, thereby preventing temperature concentration and cracking without a remarkable decrease in specific surface area [11–14]. Mechanical strength and resistance to stress can be optimized by controlling the loading of nanoparticles located inside the alumina pore, and the hydrazine decomposition rate can be changed to the desired extent [15–16]. Thus, adjusting the loading of nanoparticles, including the amount of loading on the catalyst, is paramount important in the reactor performance characteristics, because the catalyst activity of Ir nanoparticles depends on the order of atoms, crystal faces, and morphology [17].

As the nanoparticles increase, a high local concentration of products is created on the surface, leading to osmotic gradient and fluid velocity [18–21]. The movement speed of hydrazine is strongly dependent on the surface conditions of the catalyst [22]. The diffusion of hydrazine and directional mobility of the product can be controlled to improve the efficiency of reactors. To improve the resistance of Ir catalysts in gasification working conditions, a few studies have been conducted [23–25], but including an additive or changing the carrier of a catalyst such as carbon-based support does not persist under the working conditions of the reactor at high temperatures [7,26–27]. To date, no study has compared the hydrazine decomposition process on Ir catalysts with different percentages of active phase at atmospheric pressure and high-pressure reactors. Using various Ir loadings on a sup-

Corresponding author: Zahra Amirsardari E-mail: Z.amirsardari@isrc.ac.ir
© University of Science and Technology Beijing 2021

port can be considered an attempt to replace catalysts with more economical catalysts containing less than 30wt% Ir for different purposes, such as time period or modification of catalyst structures, at laboratory scale. For different life durations (short or long life system), the cost consideration of the catalyst is important [28]. For design optimization, the low weight percentages of catalysts implemented for modifying the systems are intended to reduce cost of hydrazine catalysts in research.

The purpose of the present investigation was to modify the activity and reaction rate of Ir catalysts with load contents (10wt%, 20wt%, and 30wt%) at atmospheric pressure and in a high-pressure laboratory reactor. The dispersion and particle size changes were the most effective factors of the catalysts as a result of this research. The present study focuses on the decomposition of hydrazine with two specific purposes: (1) comparison of decomposition reaction rates for various percentages of Ir catalysts and (2) observation of released gas parameters that affect system performance. To survey the first steps of hydrazine decomposition in particular and compare three types of catalysts tested, we used a self-designed laboratory reactor at atmospheric and high pressures. This study is a new economical approach with excellent activity at low Ir loading in the operating reactor.

2. Experimental

2.1. Preparation of catalysts

The Ir catalysts were prepared by wetness impregnation of dihydrogen hexachloroiridate (IV) hydrate ($H_2IrCl_6{\cdot}xH_2O$, Sigma–Aldrich) in a water-based solution onto the surface of gamma-alumina (the surface area based on Brunauer–Emmet–Teller method, S_{BET} = 160 $m^2{\cdot}g^{-1}$; 10–14 mesh; homemade product). The Ir loading of the catalysts was controlled at 10wt%, 20wt%, and 30wt% of support. After the deposition of Ir, the catalysts were dried in an oven under vacuum at 80°C for 24 h, and then calcined at 400°C for 3 h. Finally, H_2-reduction of catalysts at 400°C led to the formation of small Ir crystallites. The catalysts with load contents of 10wt%, 20wt%, and 30wt% were denoted as 10Ir, 20Ir, and 30Ir, respectively. The impregnation steps were repeated two, four, and six times (5wt% of Ir for each run) for the 10Ir, 20Ir, and 30Ir catalysts, respectively. To avoid the agglomeration of nanocrystals in the 30wt% Ir catalyst, we used 2,4-pentanedione (acetylacetone) stabilizer in the synthesis process denoted as 30Ir-S. The catalysts were used in decomposition of hydrazine monohydrate ($N_2H_4{\cdot}H_2O$, Merck).

2.2. Characterization of catalysts

The microstructures of Ir nanoparticles were examined by field emission scanning electron microscopy (FESEM; MIRA3 Tescan) and high-resolution transmission electron microscopy (HRTEM; FEI Tecnai F20). The surface areas of the catalysts were measured based on Brunauer–Emmet–Teller (BET; BELSORP-Mini, MicrotracBel) method by preconditioning at 150°C in continuously flowing inert gas for 5 h. The catalytic activities of Ir catalysts were determined by measuring the amount of gases generated by the decomposition of hydrazine monohydrate in the self-designed laboratory reactor. The sealed stainless steel reactor equipped with temperature and pressure sensors and three valves including injection, gas outlet, and safety valve was kept in a water bath to maintain the reaction temperature at 25°C. Then, 100 mg of Ir catalyst was kept inside the decomposition vessel and 10 mL of hydrazine monohydrate was added from the injection syringe by opening the gas outlet valve. The generated gases were then passed through a trap containing 1 M HCl to absorb ammonia (NH_3) and collected in an inverted cylinder by the water displacement method using an electronic balance. The weight data of the collector flask were automatically recorded by a computer program (one datum every 500 ms). The mole ratio of gases was calculated through the following equation:

$$\lambda = \frac{n(N_2 + H_2)}{n(N_2H_4)} \tag{1}$$

where λ is the molar ratio; $n(N_2 + H_2)$ is the mole number for N_2 and H_2; $n(N_2H_4)$ is the mole number for N_2H_4. The hydrogen selectivity (X) was calculated from Eq. (1) with the following equation:

$$X = \frac{3\lambda - 1}{8} \tag{2}$$

The turnover frequency (TOF) or the reaction rate (h^{-1}) in 80% conversion of hydrazine hydrate was obtained as follows:

$$\mathrm{TOF} = \frac{PV}{3n_{Ir}RTt} \tag{3}$$

where R is universal gas constant, T is reaction temperature, P is atmospheric pressure, n_{Ir} is mole number of Ir, V is volume of H_2 and N_2, and t is reaction time.

3. Results and discussion

3.1. Surface area analysis

Fig. 1 shows the adsorption–desorption isotherms of the Ir catalysts: 10Ir, 20Ir, 30Ir, and 30Ir-S. The microstructure parameters of these samples are presented in Table 1. The surface area decreases with increasing load due to the blockage of a portion of the pores with nanoparticles [29]. The increase of Ir content resulted in a decrease in the mean size of the micropores (17.2 nm for 10Ir to 15.2 nm for 30Ir-S) along with the reduction in their pore volumes. High surface aggregation degree as a result of increasing Ir loading reduced the BET surface area of 30Ir with increasing pore size compared to 30Ir-S due to less penetration into the pores. The surface area of 30Ir-S was decreased by approximately 22%

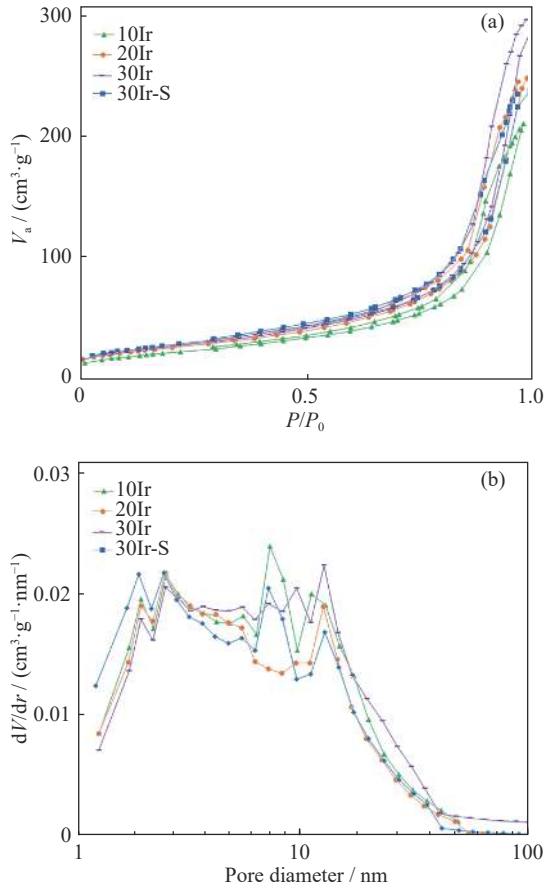

Fig. 1. (a) N_2 adsorption–desorption isotherms and (b) pore size distribution curves for Ir catalysts (V_a—Volume of gas adsorbed at standard temperature and pressure; P_0—Gas saturation pressure; r—Pore radius).

Table 1. Microstructure parameters of catalysts with different Ir contents

Catalyst	S_{BET} / ($m^2 \cdot g^{-1}$)	Pore volume / ($cm^3 \cdot g^{-1}$)	Pore diameter / nm
10Ir	126	0.48	17.2
20Ir	102	0.39	16.1
30Ir	88	0.42	18.9
30Ir-S	98	0.38	15.2

compared with that of the 10Ir sample. Reducing the surface area for 20Ir to 30Ir-S was extremely low (~4%). By adding the stabilizer to the 30wt% catalyst, the BET surface area was reduced to a very low level relative to the 20Ir catalyst through the well-controlled deposition of Ir particles onto the gamma-alumina.

3.2. High-resolution transmission electron microscopy

The TEM images were analyzed to determine the particle size. Fig. 2 shows the HRTEM images of Ir-based catalysts; these images show that Ir nanoparticles were distributed homogeneously on the gamma-alumina granular support in 10Ir, 20Ir, and 30Ir-S. However, due to the high loading of Ir particles in Ir30, the catalysts showed a tendency to aggregate, as marked in Fig. 2(c), but single particles could still be identified. The average nanoparticle size of four catalysts was measured at 2–3 nm by TEM observation. The Ir nanoparticle size almost remained constant with increasing load, which may be due to avoidance of the agglomeration and sintering. As higher catalytic activity is obtained by higher active phase of Ir nanoparticle sizes [30], these nanoparticles increase the surface area with a high number of active sites in 30wt% to promote the catalytic decomposition of hydrazine.

3.3. FESEM analysis

The surface of each catalyst was observed by FESEM images shown in Figs. 3(a) and 3(b). The growth and dispersion of Ir particles occur during the process at all available surfaces. The dispersion depends on the Ir loading in which gamma-alumina surface with a higher Ir loading shows a higher degree of coating and penetration in the pores. The nanoparticle size in all three weight percentages remained nearly constant with the control on the number of impregnation steps. However, an increase in Ir loading of the 30Ir catalyst would normally be expected to increase the low aggregation in which smaller particle size and greater distance between particles can be controlled by using a stabilizer in the 30Ir-S catalyst [31]. In addition, elemental mapping of the Ir active phase showed proper dispersion at all loadings, as shown in Fig. 3(c). The 30Ir-S catalyst should be more efficient with improved performance than the 10Ir catalyst by covering a larger surface.

3.4. Hydrazine decomposition at atmospheric pressure

The laboratory reactor at atmospheric pressure converts hydrazine monohydrate into N_2, NH_3, and a small amount of H_2 at low temperature. Although expected at high pressure in the reactor, a greater conversion of ammonia occurs with high operating temperature. Fig. 4(a) shows the time course profiles of four catalysts. The activities of 20Ir and 30Ir were higher than that of 10Ir. The level of catalyst activity varied with the loading and surface concentration of Ir and the percentage of the active phase. The 30Ir catalyst showed a sharp decrease due to the decrease in effective active surface area compared with that of the 20Ir catalyst. The 10Ir catalyst exhibited the lowest activity because of the low percentage of active phase. Based on the catalytic activity, the well-loaded Ir species can increase the activity, so that in 30Ir-S, activity was increased compared with that in 30Ir.

The content of Ir is important, but the effects of the impregnation step number and stabilizer are also dramatic. A difference existed in reaction rate (TOF) among the four types of catalysts studied, that is, Ir particles in 30Ir-S account for approximately 26% of magnitude more than Ir particles with a similar size in 10Ir. Increasing the conver-

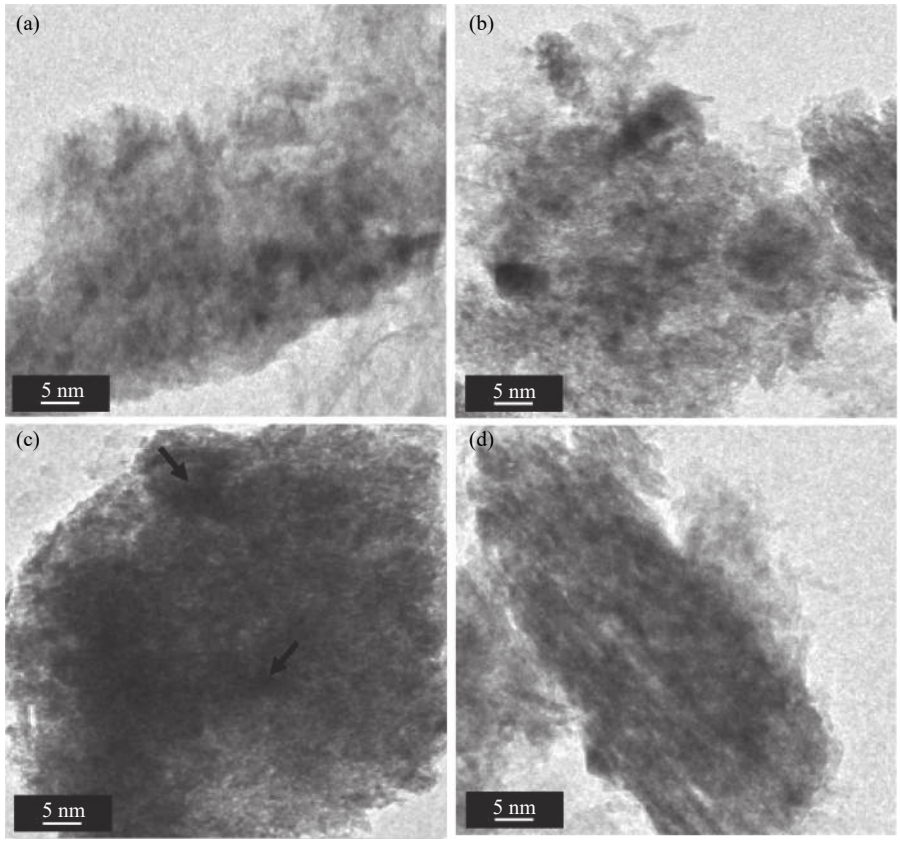

Fig. 2. HRTEM images of (a) 10Ir, (b) 20Ir, (c) 30Ir, and (d) 30Ir-S catalysts.

sion rate in the 30Ir-S catalyst results in effective distribution of the nanoparticles on the support surface. Fig. 4(b) indicates that a rate of 220 h^{-1} can be obtained for 30Ir-S with higher selectivity of hydrogen production compared with 10Ir, 20Ir, and 30Ir. As proven in previous research, Ir nanoparticles are active centers of intermediate ammonia decomposition [32]. Therefore, the higher Ir loading in 30Ir-S on the alumina support had greater selectivity of approximately 27%. Thus, with the increase of Ir content, NH_3 conversion to H_2 and N_2 increased. However, the exact decomposition mechanism of hydrazine over Ir catalysts is complex and has not been clearly defined. In general, the intramolecular nitrogen–nitrogen bond breaks more easily than the nitrogen–hydrogen bond, and NH_2 radicals (amide) can be generated on Ir. Amide radicals can be converted to the hydrogen atoms of hydrazine or lead to the formation of N_2 and NH_3 molecules [33].

Comparing reaction rates in the case of catalytic reactions determines the number of available active phases because of the parameters related to synthesis conditions, effect of agglomeration, particle size, and other factors. In this study, we have conducted the catalysts on the same support under the response of the rates with Ir mass and under the penetration of particles. The higher rate of 30wt% of Ir recorded in this study demonstrates that the 30Ir-S catalyst is a candidate. In addition, 20wt% of Ir catalyst can be a substitute in bed optimization to reduce the cost of the hydrazine catalyst.

3.5. Hydrazine decomposition at high pressure

Effect of Ir loading on catalyst performance was also investigated at high pressure in the laboratory reactor. The decomposition properties of hydrazine were different under different bed conditions. The catalytic bed was filled with the 10Ir, 20Ir, and 30Ir-S catalyst granules. Decomposition starts quickly when hydrazine is injected into the reactor and contacts with the Ir catalyst. Consequently, the pressure in the chamber increases immediately, and then reaches a maximum value. Fig. 5 compares the behaviors of these catalysts in 200 s. Chamber pressures reached a steady value within a short period in the three catalysts. The faster the decomposition of hydrazine, the faster the increase of the chamber pressure. These results indicate that all three catalysts are effective for the decomposition of hydrazine in a short period. Thus, no clear variation was observed between the stable-state pressures for all catalysts at approximately 1.5 MPa. Furthermore, the temperatures were stable at approximately 800°C in the catalyst bed, which wa greatly similar for all the three catalysts, as shown in Fig. 5. The dissociation of the ammonia produced from the decomposition of hydrazine to H_2 and N_2 is endothermic. Thus, the amount of ammonia conversion is a parameter that affects the temperature of the reactor. As shown in Figs. 5(a)–5(c), the temperatures of all

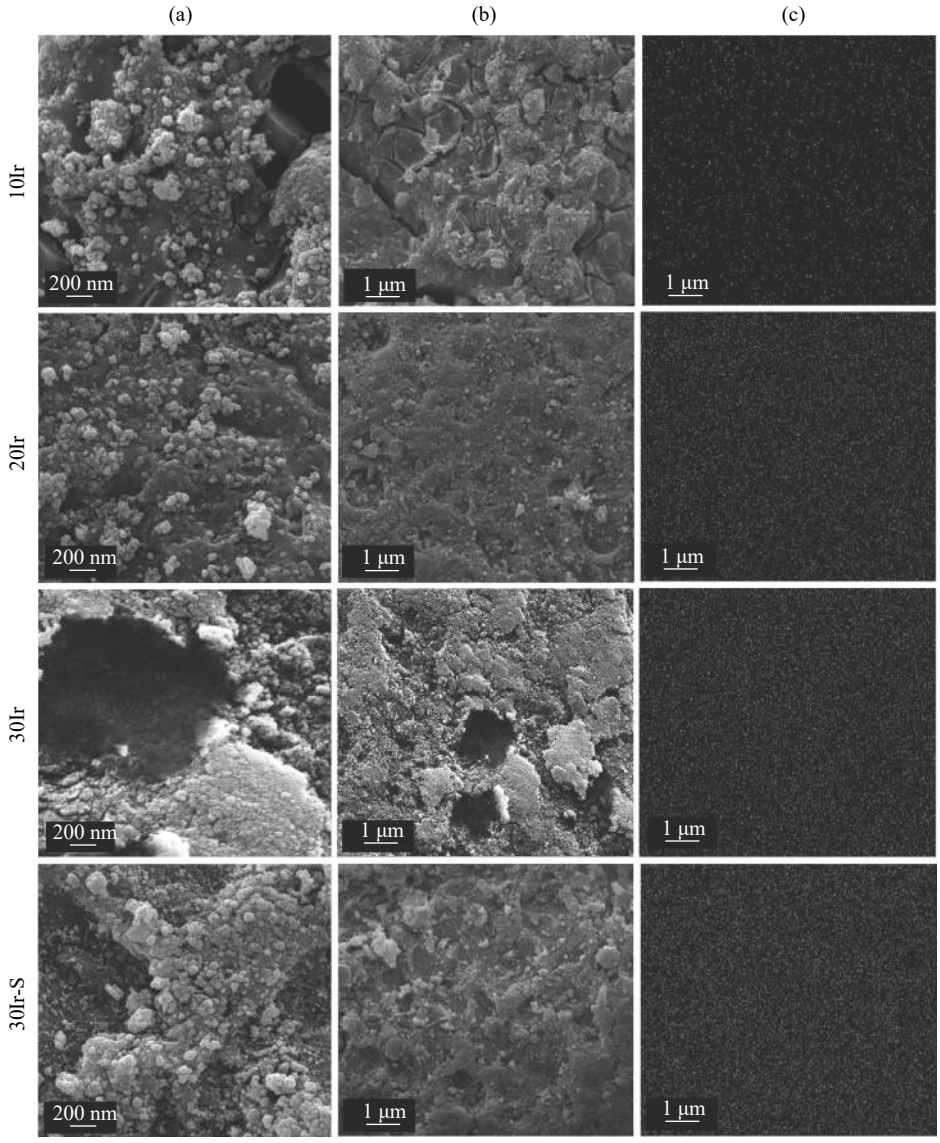

Fig. 3. (a, b) FESEM images of catalysts with different percentages of iridium nanoparticles; (c) iridium mapping images obtained from (b).

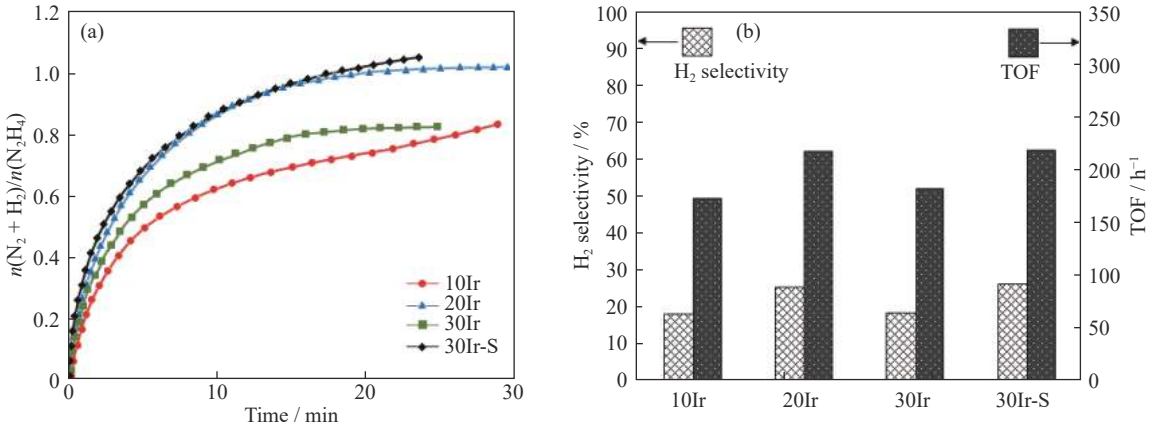

Fig. 4. (a) Hydrazine monohydrate decomposition curves and (b) comparison of H_2 selectivity and TOF of Ir catalysts at atmospheric pressure in laboratory reactor.

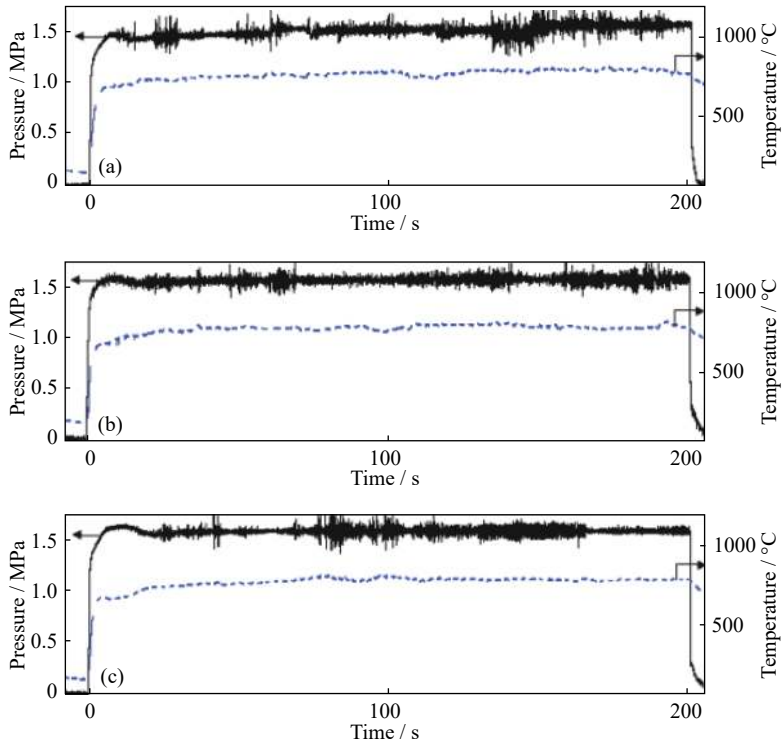

Fig. 5. Performances (pressure and temperature) of (a) 10Ir, (b) 20Ir, and (c) 30Ir-S catalysts at high pressure in laboratory reactor.

the three catalysts increased when N_2H_4 molecules decomposed and then finally rose to a stable level. The results suggest that the ammonia conversions were constant across all of the three catalysts [34]. No change in steady-state properties was observed due to the similarity in ammonia dissociation as an effective function in all the three catalysts.

The mass loss of Ir catalyst measured after the test was defined as the weight difference of the catalyst in the reactor (Table 2). Catalyst of 30Ir-S presented the smallest mass loss of approximately 2% of initial weight, while the 10Ir and 20Ir catalysts had mass losses of approximately 4% and 3%, respectively. Interestingly, the mass losses of catalysts were below 4% in different percentages of Ir.

Table 2. Catalyst properties with different Ir contents at high pressure test

Catalyst	Mass loss / %	Pressure / MPa	Temperature / °C	Velocity / ($m \cdot s^{-1}$)
10Ir	4.1	1.55	780	1300
20Ir	3	1.58	790	1314
30Ir-S	2.4	1.56	785	1303

The velocity was determined by the degree of ammonia dissociation in the second reaction of N_2H_4 decomposition. The characteristic velocity values with catalysts, including 10wt%, 20wt%, and 30wt% of Ir, were observed at 1300, 1314, and 1303 m/s, respectively. No significant difference was observed in the characteristic properties among the three catalysts. Thus, all these catalysts can be used to address the economic cost and short operating time.

4. Conclusion

The approach presented in this paper aims to improve the design and optimize the catalyst-loading level with high catalytic activity for various purposes of hydrazine decomposition such as electronic structures. The catalysts with 20wt% and 30wt% Ir on gamma-Al_2O_3 in the laboratory-scale testing showed a higher decomposition rate, and leaded to a higher amount of gaseous products, thereby providing the most efficient decomposition process. Properly controlling the loading with stabilizer can positively and significantly affect the catalytic efficiency. However, no significant difference was observed in the final characteristics for different loading levels of catalysts at high pressure. Therefore, the Ir-based catalysts with low loading are promising candidates for hydrazine decomposition for some purposes such as the portable electronic devices because of their low cost, high activity, strong mechanical strength, and fast preparation. Using different Ir loadings can be an approach to replace catalysts for some purposes such as a specific time period with cost-effective systems.

References

[1] I. Ali, K. AlGhamdi, F.T. Al-Wadaani, Advances in iridium nano catalyst preparation, characterization and applications, *J. Mol. Liq.*, 280(2019), p. 274.

[2] P. McRight, C. Popp, C. Pierce, A. Turpin, W. Urbanchock, and M. Wilson, Confidence testing of Shell-405 and S-405 catalysts in a monopropellant hydrazine thruster, [in] *41st AIAA/ASME/SAE/ASEE Joint Propulsion Conference & Exhibit*, Tucson, Arizona, 2005.

[3] P.X. Zhang, Y.G. Wang, Y.Q. Huang, T. Zhang, G.S. Wu, and J. Li, Density functional theory investigations on the catalytic mechanisms of hydrazine decompositions on Ir(111), *Catal. Today*, 165(2011), No. 1, p. 80.

[4] S. Mary, C. Kappenstein, S. Balcon, S. Rossignol, and E. Gengembre, Monopropellant decomposition catalysts. I. Ageing of highly loaded Ir/Al_2O_3 catalysts in oxygen and steam. Influence of chloride content, *Appl. Catal. A*, 182(1999), No. 2, p. 317.

[5] A.E. Makled and H. Belal, Modeling of hydrazine decomposition for monopropellant thrusters, [in] *13th International Conference on AEROSPACE SCIENCES & AVIATION TECHNOLOGY, ASAT-13*, Cairo, 2009.

[6] Z. Amirsardari, R.M. Aghdam, M. Salavati-Niasari, and S. Shakhesi, Facile carbothermal reduction synthesis of ZrB_2 nanoparticles: The effect of starting precursors, *Mater. Manuf. Processes*, 31(2016), No. 2, p. 134.

[7] Z. Amirsardari, R.M. Aghdam, M. Salavati-Niasari, and S. Shakhesi, Preparation and characterization of a novel heteronanostructure of zirconium diboride nanoparticle-coated multiwalled carbon nanotubes, *RSC Adv.*, 4(2014), No. 106, p. 61409.

[8] Z. Amirsardari, R.M. Aghdam, M. Salavati-Niasari, and M.R. Jahannama, The effect of starting precursors on size and shape modification of ZrB_2 ceramic nanoparticles, *J. Nanosci. Nanotechnol.*, 15(2015), No. 12, p. 10017.

[9] G. Fujii, D. Goto, H. Kagawa, S. Murayama, K. Kajiwara, H. Ikeda, N. Shinozaki, T. Nagao, N. Morita, and E. Yabuhara, The development results of the long life 1N hydrazine monopropellant thruster, *J. Space Technol. Sci.*, 28(2013), No. 1, p. 1_37.

[10] C.H. Hwang, S.N. Lee, S.W. Baek, C.Y. Han, S.K. Kim, and M.J. Yu, Effects of catalyst bed failure on thermochemical phenomena for a hydrazine monopropellant thruster using Ir/Al_2O_3 catalysts, *Ind. Eng. Chem. Res.*, 51(2012), No. 15, p. 5382.

[11] G. Groppi, G. Airoldi, C. Cristiani, and E. Tronconi, Characteristics of metallic structured catalysts with high thermal conductivity, *Catal. Today*, 60(2000), No. 1-2, p. 57.

[12] R.A. Mischke and J.M. Smith, Thermal conductivity of alumina catalyst pellets, *Ind. Eng. Chem. Fundamen.*, 1(1962), No. 4, p. 288.

[13] N.P. Padture, Advanced structural ceramics in aerospace propulsion, *Nat. Mater.*, 15(2016), No. 8, p. 804.

[14] S. Kang, D. Lee, and S. Kwon, Lanthanum doping for longevity of alumina catalyst bed in hydrogen peroxide thruster, *Aerosp. Sci. Technol.*, 46(2015), p. 197.

[15] K.-W. Yao, S. Jaenicke, J.-Y. Lin, and K.L. Tan, Catalytic decomposition of nitrous oxide on grafted $CuO/\gamma\text{-}Al_2O_3$ catalysts, *Appl. Catal. B*, 16(1998), No. 3, p. 291.

[16] I.J. Jang, H.S. Shin, N.R. Shin, S.H. Kim, S.K. Kim, M.J. Yu, and S.J. Cho, Macroporous–mesoporous alumina supported iridium catalyst for hydrazine decomposition, *Catal. Today*, 185(2012), No. 1, p. 198.

[17] M.L. Cui, Y.S. Chen, Q.F. Xie, D.P. Yang, and M.Y. Han, Synthesis, properties and applications of noble metal iridium nanomaterials, *Coord. Chem. Rev.*, 387(2019), p. 450.

[18] I. Ali, Z.A. Alothman, and A. Alwarthan, Supra molecular mechanism of the removal of 17-β-estradiol endocrine disturbing pollutant from water on functionalized iron nano particles, *J. Mol. Liq.*, 241(2017), p. 123.

[19] I. Ali, Microwave assisted economic synthesis of multi walled carbon nanotubes for arsenic species removal in water: Batch and column operations, *J. Mol. Liq.*, 271(2018), p. 677.

[20] I. Ali, O.M.L. Alharbi, Z.A. Alothman, and A. Alwarthan, Facile and eco-friendly synthesis of functionalized iron nanoparticles for cyanazine removal in water, *Colloids Surf. B*, 171(2018), p. 606.

[21] I. Ali, A.A. Basheer, A. Kucherova, N. Memetov, T. Pasko, K. Ovchinnikov, V. Pershin, D. Kuznetsov, E. Galunin, V. Grachev, and A. Tkachev, Advances in carbon nanomaterials as lubricants modifiers, *J. Mol. Liq.*, 279(2019), p. 251.

[22] W. Gao, A. Pei, R.F. Dong, and J. Wang, Catalytic iridium-based Janus micromotors powered by ultralow levels of chemical fuels, *J. Am. Chem. Soc.*, 136(2014), No. 6, p. 2276.

[23] R. Vieira, C. Pham-Huu, N. Keller, and M.J. Ledoux, New carbon nanofiber/graphite felt composite for use as a catalyst support for hydrazine catalytic decomposition, *Chem. Commun.*, (2002), No. 9, p. 954.

[24] V. Prasad and M.S. Vasanthkumar, Iridium-decorated multiwall carbon nanotubes and its catalytic activity with Shell 405 in hydrazine decomposition, *J. Nanopart. Res.*, 17(2015), No. 10, art. No. 398.

[25] N. Firdous, N.K. Janjua, I. Qazi, and M.H.S. Wattoo, Optimal Co–Ir bimetallic catalysts supported on $\gamma\text{-}Al_2O_3$ for hydrogen generation from hydrous hydrazine, *Int. J. Hydrogen Energy*, 41(2016), No. 2, p. 984.

[26] J. Luo, M.M. Maye, V. Petkov, N.N. Kariuki, L.Y. Wang, P. Njoki, D. Mott, Y. Lin, and C.J. Zhong, Phase properties of carbon-supported gold–platinum nanoparticles with different bimetallic compositions, *Chem. Mater.*, 17(2005), No. 12, p. 3086.

[27] T. Cordero-Lanzac, R. Palos, J.M. Arandes, P. Castaño, J. Rodríguez-Mirasol, T. Cordero, and J. Bilbao, Stability of an acid activated carbon based bifunctional catalyst for the raw bio-oil hydrodeoxygenation, *Appl. Catal. B*, 203(2017), p. 389.

[28] J.N. Hinckel, J.A.R. Jorge, T.G.S. Neto, M.A. Zacharias, and J.A.L. Palandi, Low cost catalysts for hydrazine monopropellant thrusters, [in] *45th AIAA/ASME/SAE/ASEE Joint Propulsion Conference & Exhibit*, Denver, Colorado, 2009.

[29] Z.M. Zhang, X. Hu, J.J. Li, G.G. Gao, D.H. Dong, R. Westerhof, S. Hu, J. Xiang, and Y. Wang, Steam reforming of acetic acid over Ni/Al_2O_3 catalysts: Correlation of nickel loading with properties and catalytic behaviors of the catalysts, *Fuel*, 217(2018), p. 389.

[30] D.M. Doyle, G. Palumbo, K.T. Aust, A.M. El-Sherik, and U. Erb, The influence of intercrystalline defects on hydrogen activity and transport in nickel, *Acta Metall. Mater.*, 43(1995), No. 8, p. 3027.

[31] Z. Amirsardari, A. Dourani, M.A. Amirifar, N.G. Massoom, and M.R. Jahannama, Controlled attachment of ultrafine iridium nanoparticles on mesoporous aluminosilicate granules with carbon nanotubes and acetyl acetone, *Mater. Chem. Phys.*, 239(2020), art. No. 122015.

[32] L. Li, X.D. Wang, X.Q. Zhao, M.Y. Zheng, R.H. Cheng, L.X. Zhou, and T. Zhang, Microcalorimetric studies of the iridium catalyst for hydrazine decomposition reaction, *Thermochim. Acta*, 434(2005), No. 1-2, p. 119.

[33] S.G. Pakdehi and M. Rasoolzadeh, Comparison of catalytic behavior of iridium and nickel nanocatalysts for decomposition of hydrazine, *Procedia Mater. Sci.*, 11(2015), p. 749.

[34] D.I. Han, C.Y. Han, and H.D. Shin, Empirical and computational performance prediction for monopropellant hydrazine thruster employed for satellite, *J. Spacecraft Rockets*, 46(2009), No. 6, p. 1186.